PUBLICATIONS OF THE ASTRONOMICAL SOCIETY OF THE PACIFIC
102: 1064–1076, September 1990

MILLIPOL, A MILLIMETER/SUBMILLIMETER WAVELENGTH POLARIMETER: INSTRUMENT, OPERATION, AND CALIBRATION

DAN P. CLEMENS

Astronomy Department, Boston University, 725 Commonwealth Avenue, Boston, Massachusetts 02215

ROBERT W. LEACH

Department of Astronomy, PA-210, San Diego State University, San Diego, California 92182

RICHARD BARVAINIS

Haystack Observatory, NEROC, Route 40, Westford, Massachusetts 01886

AND

BRIAN D. KANE

Astronomy Department, Boston University, 725 Commonwealth Avenue, Boston, Massachusetts 02215

Received 1990 January 8, revised 1990 June 20

ABSTRACT

An instrument capable of measuring the polarization characteristics of weakly polarized, cold dust at millimeter and submillimeter wavelengths is presented in detail. This instrument consists of a rotating half-wave plate and the data-collection electronics, computers, and software necessary to convert existing millimeter-wave coherent detection receivers into a sensitive polarimeter. The operation and calibration of this polarimeter at a wavelength of 1300 μm, configured for the NRAO 12-meter telescope, are discussed with particular emphasis placed on characterization of the instrumental polarization. Deep observations of Jupiter using this instrument revealed a main-beam instrumental polarization at, or below, the 0.2% level. Lunar limb observations revealed a sidelobe polarization sensitivity, in the range 0.25%–1.0%. Further, through these efforts we have detected the nonthermal polarized flux from Jupiter at a level of about 0.04% (~ 1.5 Jy) of the thermal flux. Astronomical polarization measurements to 0.03% are possible, limited by the uncertainties in the instrumental polarization. This instrument has been primarily employed to measure and map magnetic-field directions in the very optically opaque cores of massive molecular clouds.

Key words: instrumentation–polarization–observing techniques

1. Introduction

Magnetic fields may play an important role in the star-formation process in molecular clouds. These fields may support clouds against gravitational collapse, help to order dense cloud core or protostellar disk formation, and may order or even drive the high-velocity outflows from regions of recent star formation. However, our understanding of the importance of magnetic fields in these dense regions is limited by our inability to easily probe and measure the magnetic fields there.

The obscuring dust in a molecular cloud, in concert with any associated magnetic field, induces an anisotropic absorption which is readily detected as weak linear polarization in the light from distant background stars at optical and near-infrared wavelengths. But, because the optical extinctions toward cloud cores are so huge, traditional stellar polarization mapping (e.g., Heyer *et al.* 1987) can only be performed toward molecular-cloud peripheries. However, the same dust which produces the anisotropic optical absorption is also emitting, though with characteristically cool temperatures, in the range of 10 K–50 K. This dust emission can be detected in the far-infrared, submillimeter, and millimeter wave bands via its continuum emission.

The magnetic fields in dense cloud cores have been probed at far-infrared wavelengths (100–270 μm) by Hildebrand, Dragovan, and Novak (1984), Dragovan (1986), Werner *et al.* (1988), and Novak *et al.* (1989*a*,*b*). Their technique utilized supercooled bolometer-based polarimeters in conjunction with the one-meter aperture telescope of the Kuiper Airborne Observatory (KAO). They were able to successfully detect the far-infrared

polarized emission from the Orion cloud core, Monocerotis R2, and the Galactic center region.

We have elected to pursue a ground-based effort at millimeter, and hopefully submillimeter, wavelengths. There are several advantages to this approach which counteract the much weaker fluxes emitted by the cold dust at millimeter wavelengths. First, there is a large aperture increase possible with ground-based millimeter and submillimeter telescopes compared to the KAO. Second, the angular resolution for ground-based millimeter magnetic field mapping is at least as good and can be much better than that possible at far-infrared wavelengths from the KAO. Finally, the operation of a polarimeter and data-collection equipment is much simpler, more reliable, and more efficient when the telescope is ground based and the moving parts of the instrument are at room temperature.

In order to capitalize on these advantages, we built a polarimeter for a wavelength of 1300 μm and operated it on the 12-meter NRAO[1] telescope (Barvainis, Clemens, and Leach 1988, hereafter BCL). This instrument has undergone significant evolution during the three years of its use. In this paper we present the current version of MILLIPOL (for *Milli*meter *Pol*arimeter) and discuss our efforts to operate it and to calibrate the observations.

Using this instrument we have (1) detected, for the first time at this wavelength, the nonthermal emission from Jupiter (discussed in Section 4, below); (2) made a flux-limited polarimetric map of the Orion molecular cloud core (Leach *et al.* 1990); (3) detected polarized dust emission from several other molecular cloud cores (Clemens *et al.* 1990); and (4) monitored the polarization properties of two bright quasars.

In the following sections we discuss the basic design of MILLIPOL, some practical mitigating issues and their solutions, the details of the operation of the instrument, and our attempts to determine the instrumental calibration quantities. The derived values for the main-beam instrumental polarization are surprisingly low, ~ 0.2%, yet are well determined. Finally, we show how our effort to characterize the instrumental polarization led to the detection of polarized flux from Jupiter, increasing the maximum frequency for detection of the nonthermal radiation of Jupiter by more than a factor of ten.

2. The MILLIPOL Instrument

In the following description of our instrument we begin by presenting the basic theory behind polarimetric observing with a half-wave plate. Next, we list some of the practical problems which must be overcome in order to perform accurate polarimetry at millimeter and submillimeter wavelengths toward molecular cloud core regions (regions exhibiting both weak signals and low polarizations). Finally, we discuss the features of the MILLIPOL instrument which attempt to address, alleviate, or eliminate these problems. For the bravest of readers, we include in the Appendix a detailed discussion of the hardware tradeoffs and settings necessary to making MILLIPOL a working, accurate instrument on the 12-meter telescope.

2.1 *Theory of Operation*

In Figure 1 we show a schematic diagram of the MILLIPOL and NRAO 12-meter elements, identifying which belong to MILLIPOL and which to the 12 meter. The radiation collected by the telescope, containing the desired weakly polarized component, traverses a half-wave plate. The position angle of the linearly polarized component is rotated by the half-wave plate, by an angle equal to twice the offset angle of the half-wave plate with respect to its zero phase position. The wave is split into its horizontal and vertical components by the fixed wire grids and enters the cooled receiver dewar to be mixed to lower (IF) frequencies by the two independent Schottky receivers. The values of the signal polarization (percentage polarization and position angle on the sky) are obtained from the multiple measurements of the signal strength in the vertical and horizontal receivers as a function of the offset angle of the half-wave plate. The modulated signals take the form of sinusoids of amplitude related to the half-wave plate offset angle, with four full cycles of the sinusoids for every full revolution of the half-wave plate. The polarization percentage is obtained from a comparison of the amplitude of the sinusoids to the total flux amplitude. The position angle is obtained from the phase angle offset of the sinusoid relative to the zero of phase angle for the half-wave plate.

2.2 *Practical Problems and Concerns*

In addition to the theoretical aspects, a working polarimeter system is typically dominated by practical considerations, such as sky and telescope effects, effects introduced by the half-wave plate rotation and efficiency, and strategies for optimal data collection and calibration. We briefly list the concerns which were most important in influencing the details of the MILLIPOL design.

In the first place, the sky transmission varies quickly with time at millimeter wavelengths, and even more so at submillimeter wavelengths. There seem to be at least two relevant time scales for the variation. The longest time scale is that associated with large changes in the atmospheric attenuation, due to changes in the amount of precipitable water vapor. The time scale for a factor of two change in the opacity can be as long as many hours or as short as several minutes during poor or marginal weather. The more important time scale, however, is a photometric one, which seems to require sky chopping at least at

[1]The National Radio Astronomy Observatory is operated by the Association of Universities for Research in Astronomy, Inc., under contract with the National Science Foundation.

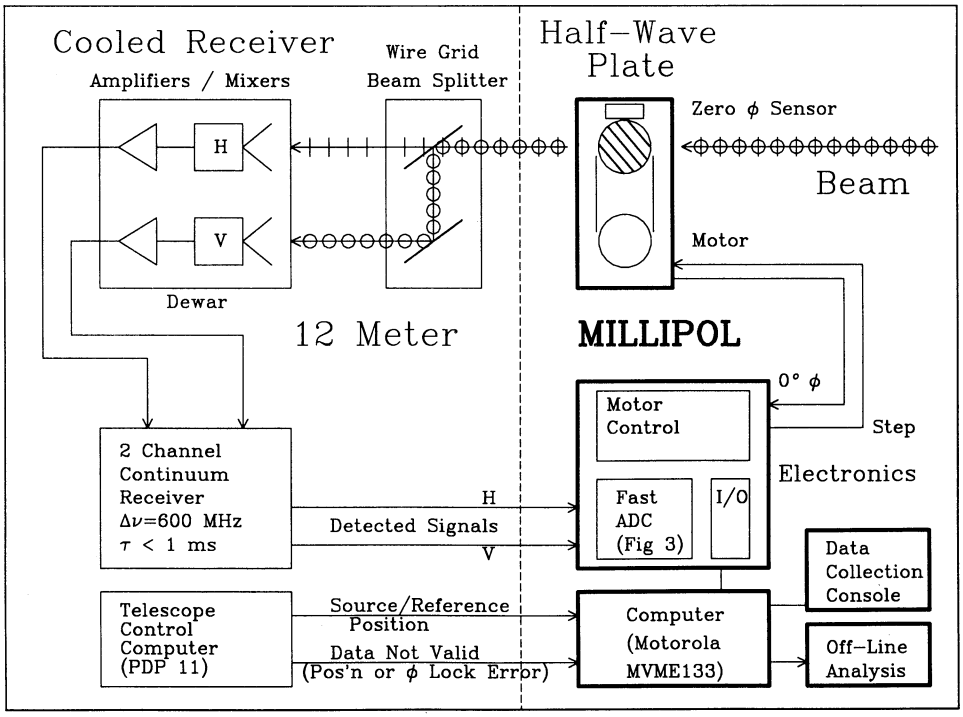

FIG. 1–Block diagram of the MILLIPOL components configured on the NRAO 12-meter telescope system. The MILLIPOL components are shown to the right of the vertical dashed line; the 12-meter components are to the left. The beam from the telescope passed through the rotating rexolite half-wave plate before being analyzed by the wire grids, mixed in the cooled receiver, and detected by the continuum receiver. The MILLIPOL electronics and computer system synchronously integrated the continuum receiver output during small intervals of the half-wave plate rotation. Angular synchronization was provided by a zero phase signal ("0° φ") generated by an optical interrupter.

the 5–10 Hz rate to remove noise generated by quick changes in the level of atmospheric emission at 1300 μm. Accurate polarimetry is not intrinsically immune to this short-term, sky-noise problem. For MILLIPOL we designed the instrument to be able to collect one full modulation cycle of signal polarization every 40 milliseconds. This fast polarization modulation rate effectively "freezes" the sky variation during the measurement, similar to the way fast beam chopping freezes the sky variation for photometric measurements.

The levels of the expected polarization signals also posed practical problems. Because the millimeter flux due to thermal dust emission from warm molecular cloud cores is very small, and the degree of polarization is also very small, the measurements are strongly limited by low signal-to-noise ratio and pose dynamic range and linearity problems for the processing electronics. Even for a relatively bright source like the Orion cloud core, the unpolarized flux represents only 0.05% of the receiver plus sky noise. Inclusion of the less than 3% polarization of that flux and the desire to precisely measure the polarization drives the dynamic range to almost 10^6.

Additionally, the MILLIPOL instrument needed to accept and process information from the telescope control computer system in order to effectively "shutter" the data collection. This information enabled the instrument to halt data collection if wind blew the telescope away from its commanded sky position or if the receiver local oscillator phase-lock-loop system became unlocked. MILLIPOL also needed to be informed whenever the telescope switched from source to reference positions. As a practical problem, the 12-meter telescope system only updated such information at a 10 Hz rate, while MILLIPOL collected data at better than a 1 kHz rate. Another consideration which required monitoring was possible mechanical failure of the rotating half-wave plate. If the plate motor drive were to quit, the data collection needed to be halted.

Finally, the cost of the project had to be essentially zero. Many of the MILLIPOL solutions to other concerns were strongly influenced by this rather practical limit (introducing such things as software solutions to hardware problems).

2.3 *MILLIPOL Design*

In the sections which follow we describe the components of MILLIPOL, giving particular attention to solutions to the problems raised in the preceding section. The MILLIPOL instrument hardware additions to existing telescope and receiver combinations consist of the rotating half-wave plate, the data-collection computer, and the analog and digital electronics system.

2.3.1 *Half-Wave Plate*

The details of the design and construction of grooved,

millimeter-wavelength rexolite (Plexiglass) half-wave plates may be found in Barvainis (1984). Our half-wave plate is unchanged from that used by BCL, though it is rotated about four times faster to achieve polarization modulation of the incoming signal polarization at something faster than 25 Hz to effectively freeze the sky during a measurement. The rexolite half-wave plate was characterized during the 1989 observing session to exhibit an insertion loss of 15% (0.71 dB) and, during previous laboratory experiments, to have a polarization efficiency of 95% ± 5%. It was designed to pass a 9-cm beam, to operate at room temperature, and to be placed in the optical path after the ambient temperature chopper calibration vane, and before the beam-splitting wire grids. The plate makes 200 discrete steps per revolution, with a dwell time at any one position angle of 800 μs, to generate a 6.25 Hz half-wave plate rotation rate.

2.3.2 *Electronics*

The analog and digital signal-processing electronics were completely changed from those discussed in BCL. The new set of electronics was designed specifically for MILLIPOL with few compromises—the electronics were designed to squeeze the maximum performance out of the polarimeter without introducing spurious effects. The main task of these electronics was to integrate and digitize the modulation induced by the half-wave plate on the signal received by the NRAO dual-channel cooled Schottky mixers and detected by the NRAO continuum receiver. Additionally, the electronics system buffered information between the data-collection computer and both the half-wave plate motor system and the telescope control computer. The electronics were designed to perform an integration and digitization at the half-wave plate step rate (> 1000 Hz) for both horizontal and vertical receiver channels, with an accuracy of 16 bits, and to oversample the receiver noise to avoid digitization noise in subsequent scan averages. This data-collection rate is more than one hundred times faster than the normal data-collection rate of the NRAO 12-meter telescope system, hence the need to build custom electronics. Other detailed design considerations for the electronics subsystems are described in the Appendix.

2.3.3 *Computer*

In the overall design of MILLIPOL, we chose to deeply embed the computer into the system. The computer issued all of the low-level commands to cause the electronics system to reset integrators, start the analog-to-digital conversion process, hold the analog signal at its current level, and multiplex the digitized data onto the narrow data pathway between the electronics and the computer. The computer also issued the step instructions to the half-wave plate motor and monitored the telescope-control-computer telescope position and receiver phase-lock-loop status values. And, during all of this low-level activity, the computer ran high-level FORTRAN-based code to oversee the data collection, accumulation, and logging.

The problem of the long delay time between an external activity (telescope position change, or local oscillator phase-lock-loop error) and the reporting of that activity by the telescope control computer, by up to 0.1 sec, was solved by keeping a large buffer for newly collected data in our data-collection computer. Before the new data for a 0.1 second period (somewhat more than 200 measurements) were added to the accumulating data, the telescope status lines were polled. If there had been a change, the new data buffer was flushed. If no change had occurred, and the conditions were acceptable, the new data buffer was added to the scan accumulators. Hence, data accumulation lagged 0.1 sec behind data collection and was "shuttered" based on the real-time telescope performance to reject bad data.

Mechanical failures of the half-wave plate were detected by counting step commands issued to the plate motor and sensing for too many steps between plate zero-phase conditions (detected by an optical interrupter).

2.4 *MILLIPOL Performance and Operation*

MILLIPOL was operated at the NRAO 12-meter telescope during three separate observing sessions. The initial observing run covered 1987 March 5–8. Scientific results from that run, as well as the operation of MILLIPOL, were discussed in BCL. The second observing session covered 1988 April 2–7 and the most recent observing run took place during 1989 January 19–24. In all that follows these are referred to as observing sessions in 1987, 1988, and 1989, respectively. At the telescope during the 1988 and 1989 runs, the measured system detection speed was 6 Jy $Hz^{-0.5}$, equal to the theoretical value for the 600 MHz detection bandwidth.

Observations using MILLIPOL involved several nonstandard techniques and some necessary trade-offs. We elected to modulate the signal using the half-wave plate at a fast rate (25 Hz) but to switch between source and reference positions at a slow rate (once every 30 seconds). A better approach would be to combine fast polarization modulation with fast beam chopping, at around 10 Hz, which we will try in the future. In order to overcome some of the systematics introduced by the long position-switching cycles, the reference positions were chosen to be offset from the source positions by 34^s of right ascension (30 seconds of integration plus 4 seconds of telescope moving and settling time). This had the desirable effect of allowing observations of both the source and reference positions to pass through identical air masses of the atmosphere. A marked improvement over the usual azimuth switching was noticed in the residual noise of the polarization scans. Hence, right-ascension position switching was used throughout the 1988 and 1989 observations (see acknowledgments below).

Finally, because polarization data collection by MILLIPOL occurred independently of total flux data collection by the 12-meter telescope system, cross calibration of the total and polarized flux values was required. During normal observations, the 12-meter data-collection system was used in beam-switched mode (secondary chopping) to measure the total flux for a source, and MILLIPOL was subsequently used in the position-switched mode to measure the polarized flux. The calibration of MILLIPOL fluxes was achieved by determining the mean position-switched signal difference between Jupiter and the sky and assigning the beam-switched flux for Jupiter measured by the 12-meter system immediately before or after the MILLIPOL measurements. The uncertainty introduced by this cross calibration is primarily due to the poorer total flux measurements obtained using MILLIPOL in position-switched mode. The typical uncertainty introduced is around 5%, which is usually far below the percentage polarization measurement noise for the cloud core regions. Note that there is no additional uncertainty added to the polarization position angles.

Our standard mode of observing consisted of using the 12-meter system to obtain a beam-switched total flux measurement of a source, followed by 10–12 five-minute-duration MILLIPOL scans (each consisting of five source-reference cycles of 30-second duration in each position) to determine the polarized flux. For weak sources this cycle was repeated as needed. Sky dips were performed about every 2–3 hours to establish atmospheric opacity.

Periodically, a fast serial link was used to transfer stored data from the MILLIPOL computer to a PC clone computer for off-line analysis. The PC ran a custom FORTRAN program containing routines to append observing coordinates and other pertinent information to the reconstructed raw receiver analog voltage data, to convert the analog voltages to astronomical flux values, to analyze the polarization properties of the scans, to average scans, and to plot scans. This program also computed the polarization corrections to the raw data to remove the half-wave plate offset angle effects, the parallactic angle rotation of the source with respect to the azimuth-elevation mounted receiver feed horns, and the measured instrumental polarizations (see below).

3. Instrumental Polarization

Because the percentage polarization of the molecular-cloud core regions observed was so small (typically ~ 1%), an extensive effort was undertaken to characterize the level of polarization induced by the combination of the 12-meter telescope and the MILLIPOL half-wave plate. This effort included repeated observations of the radial polarization of the limb of the Moon, extensive planetary observations, and analysis of multiple parallactic angle observations of the fairly bright, but weakly polarized, source Orion KL. The multiple methods are in good agreement, yielding a best estimate for the main-beam instrumental polarization of 0.2% with uncertainties of 0.01%–0.06%, depending on the observing run and receiver channel employed. The sidelobe polarization was measured to be in the range 0.25%–1.0%. The details of these measurements are described in what follows.

3.1 *Moon Calibration*

Observations of many positions around the limb of the Moon were obtained in six separate series of multiple polarimetric scans during the 1988 and 1989 observing runs. As discussed in BCL, regression of the observed polarization position angles of the ~1% radially polarized Moon emission (cf. Hagfors 1970 and references therein) with the position angles of the telescope beam on the limb of the Moon leads to the half-wave plate zero-phase offset angle and a slope. In all cases, the absolute value of the slope is indistinguishable from unity. The offset angle carries information about how to convert raw, observed MILLIPOL polarization position angles to absolute sky polarization position angles.

The actual process is a four-step one:

(1) Point the telescope to a Moon limb position i, whose position angle from the center of the Moon is $\mathrm{P.A.(Moon)}_i$.

(2) Use MILLIPOL to measure the polarization position angle of the Moon emission there. The polarization position angle with respect to the arbitrary zero phase of the half-wave plate is $\mathrm{P.A.(raw)}_i$.

(3) Repeat steps 1 and 2 for many other Moon limb positions. Regress the raw MILLIPOL polarization position angles with Moon limb position angles to determine the sign of the slope and the value of the offset angle as:

$$\mathrm{P.A.(Offset)} = \mathrm{P.A.(raw)} + \mathrm{slope} * \mathrm{P.A.(Moon)} \ , \quad (1)$$

where slope is +1 or −1, depending on the direction of the half-wave plate rotation.

(4) Correct later astronomical MILLIPOL observations for the half-wave plate zero-phase offset angle as:

$$\mathrm{P.A.(sky)} = \mathrm{slope} * \{\mathrm{P.A.(obs)} - \mathrm{P.A.(Offset)}\} \ . \quad (2)$$

Table 1 summarizes the six sets of Moon scans obtained in 1988 and 1989. The first two columns list the UT date and average LST for each series of scans. The numbers of scans in each series are listed in the third column, where most scans were of two-minute duration and were collected in the autoleveling mode discussed in the Appendix. Each scan was obtained toward a different Moon limb angle $\mathrm{P.A.(Moon)}_i$. Three of the Moon series had too few scans for the sidelobe analysis (see below). The remaining columns list the derived offset angles P.A.(Offset) and uncertainties for the receiver channels H and V.

There are several points to consider regarding the offset angles. First, in the table the offset angle for receiver

TABLE 1

Moon Observations

Date (U.T.)	LST (HHMM)	Scans	$\theta(H)$ (Degrees)	$\theta(V)$ (Degrees)
4/2/88	1150	13	42.65 (0.07)[a]	42.21 (0.10)
4/6/88	1705	3[b]	40.53	40.81
4/7/88	1535	2[b]	47.83	44.65
1/19/89	1030	10	30.78 (0.10)	30.09 (0.18)
1/20/89	0209	5[b]	32.40	32.19
1/20/89	1030	9	30.95 (0.14)	30.63 (0.14)

[a] Numbers in parentheses are 1 σ uncertainties in the constant fitted with the sidelobe sine wave (see Section 3.1 in text).

[b] Incomplete sampling of lunar limb position angles. Sine wave fitting was not well constrained.

channel V has been mathematically rotated by exactly 90° to give it a channel H-like reference angle to ease later data averaging. Second, the direction of half-wave plate rotation was inadvertently reversed between the two years. Since the zero of MILLIPOL angular phase (see Fig. 1) in 1988 was established by a microswitch and in 1989 by an optical interrupter, the absolute values of the offset angles should not be expected to be identical. Third, the phase of channel V relative to channel H depends on the half-wave plate rotation direction (+90° or −90°), and this has already been accounted for in the table. Finally, the H and V channels are not exactly 90° apart. The data for 1988 and 1989 yield relative offset angles of 0°.44 ± 0°.12 and 0°.50 ± 0°.14 from the 90° assumption. Taken together (since the receiver was unchanged from one year to the next), we infer a mean offset of 90°.46 ± 0°.09 for the 1988 H-V angle, and 89°.54 ± 0°.09 for the 1989 H-V angle (since the half-wave plate rotation directions were different for the two years). In all of the data presentations which follow Table 1, all V-channel data have been corrected for both the half-wave plate rotation direction and the measured offset angle relative to the channel H receiver position.

However, within each series of Moon scans, the half-wave plate zero-phase offset angles derived for each individual scan (eq. (1) above, but for each scan instead of the series regression) differ from each other by much more than their measured uncertainties. This is most likely due to a combination of the sidelobe polarization and incomplete Moon observations, as is demonstrated in the following.

The run of raw MILLIPOL polarization position angles P.A.(raw)$_i$ versus Moon limb position angle P.A.(Moon)$_i$ does not quite follow the straight-line regression discussed above. If we select the first set of Moon observations from 1989, and plot the ten *individually* derived half-wave plate zero-phase offset angles P.A.(Offset)$_i$ versus the Moon limb position angles P.A.(Moon)$_i$, Figure 2 is the result. This figure shows the V-channel data only. In addition to the data points, a best-fit sine wave is shown. The sine wave was constrained to be a two-cycle wave, but to be free in amplitude and phase. The amplitude fitted was 6°.0 ± 0°.3, and the phase was −65° ± 3°. The data values are clearly well represented by this curve.

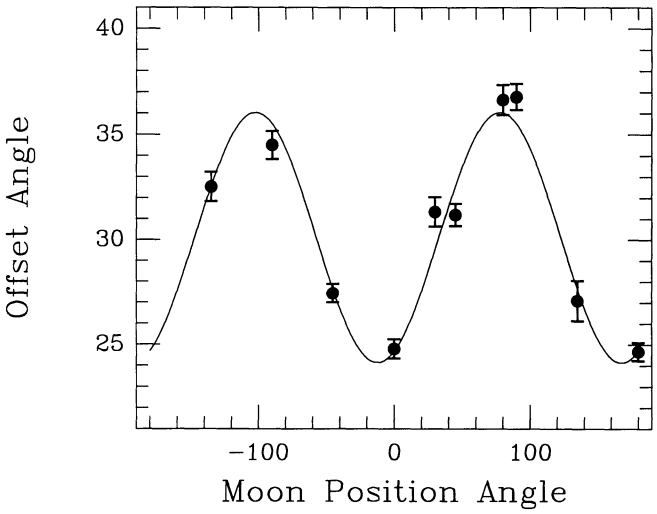

FIG. 2—Plot of the half-wave plate zero-phase offset angle P.A. (Offset) derived from the 1989 observations (first data series) versus position angle around the limb of the Moon P.A.(Moon). The curve represents the best-fit constant plus double sine wave. The sine wave with Moon position angle is most likely due to sidelobe polarization sensitivity convolved with the radial lunar polarization direction.

Such a curve could arise from an instrumental polarization. However, these data points have already been corrected for the main-beam instrumental polarization (as described in a later section). Removal of the main-beam correction shifts the phase and amplitude of the curve. The amplitude ratio between the main-beam corrected and uncorrected curves can be used to estimate the relative main-beam and sidelobe effects (see below). Hence, we identify the source of the main-beam *corrected* angular variation (e.g., Fig. 2) as being due to the polarization sensitivity of the 12-meter sidelobes which fall onto the Moon during the limb observations.

The degree of sidelobe polarization can be estimated as follows. If we treat this angular variation as arising from a variable polarization (due to the projection of the sidelobe polarization response with the radial polarization of the Moon), then we estimate the sidelobe polarization as:

$$P_{\text{SIDELOBE}} = 2\,\beta\,\eta^{-1}\,P_{\text{MOON}}\ , \qquad (3)$$

where β is the angular amplitude of the fitted sine wave in radians. The efficiency term η is the ratio of power in the sidelobes to the total power in the entire telescope beam, which for observations of the lunar limb we estimate to be about 20%. If the lunar polarization is about 1%, then $P_{\text{SIDELOBE}} \sim 1\%$ for the data shown in Figure 2. The H receiver channel showed a sine amplitude of half that in the V channel. Similar analyses of the 1988 lunar observations yield sidelobe polarizations as low as 0.25%.

For the first set of lunar observations in 1988, and the first and third set of lunar observations in 1989, enough Moon observing angles were sampled to lead to well-constrained sine-wave fitting. However, for the less-complete observations, incomplete sampling could produce angular errors by as much as 3°–6°, easily explaining the variations in offset angles seen in Table 1. Hereafter, for angular calibrations, we adopt the fitted constant terms for the Moon observations possessing sufficient angular coverage to prevent bias due to sidelobe polarization.

It should also be noted here that although the level of sidelobe polarization exceeds that of the main beam, for all of the astronomical observations the sidelobe solid angle filled by the small sources is very tiny. Hence, the sidelobe contribution to the total instrumental polarization correction is negligible for our observations to date. However, sidelobe polarization will become more important for observations obtained with higher sensitivity (bolometer-based systems) and at shorter wavelengths, where the ratio of beam to source areas becomes small.

3.2 *Direct Determination via Orion Observations*

A direct measure of the main-beam instrumental polarization can be made by observing the change of the observed Stokes parameters with parallactic angle as a source tracks across the sky. For observations using an azimuth-elevation telescope, the U and Q parameters will contain components which rotate with the source parallactic angle and can be identified as the source polarization, and components which do not rotate and can be identified as the instrumental polarization. Least-squares fitting to a run of observed U and Q with parallactic angle can be used to recover the source and instrumental polarizations (Novak *et al.* 1989*a*). Attention must be paid to the quality of the input data, however. Good sky tracks, covering large parallactic angle changes, are needed to ensure that the least-squares solutions are reasonable.

Orion KL is a good source for such a test. It is both bright (~ 45 Jy) and, compared to other H II regions, relatively highly polarized (~2.5%), making separation of the source and instrumental polarizations possible (Novak 1989*a*). Table 2 presents the results of our Orion KL reductions for 1988 and 1989. For each year, only data for a single source position, collected on a single day, and containing many scans covering a large parallactic angle range, are included. These are the best data for this test. The runs of U and Q with parallactic angle were processed by our least-squares program to yield the Table 2 information. Note that the 1988 channel V data are likely affected by saturation of the 12-bit ADC (see Appendix). In what follows, we ignore the 1988 channel V entries of the table.

First, in 1988 channel H and in 1989 channels H and V, the source polarization is readily detected and the percent polarization and position angle are in reasonable agreement. The instrumental polarizations are all comparable to their uncertainties. Because percentage polarization obeys a Ricean distribution, these results are consistent with no instrumental polarization to the uncertainty levels indicated. Hence for Orion, we do detect the source polarization, but we see no instrumental polarization above a 2σ limit of about 1%. In order to measure the instrumental polarization to a lower level, a stronger source was needed.

TABLE 2

Orion Instrumental Polarization

Year	Quantity	Channel *H*	Channel *V*
1988	P_{SOURCE}(%)	3.18 (0.89)[a]	1.70 (1.40)
	θ_{SOURCE}(°)	35 (8)	63 (20)
	$P_{INST.}$(%)	0.54 (0.89)	2.73 (1.40)
	$\theta_{INST.}$(°)	74 (29)	−43 (14)
1989	P_{SOURCE}(%)	2.02 (0.50)	1.41 (0.68)
	θ_{SOURCE}(°)	16 (7)	39 (13)
	$P_{INST.}$(%)	0.63 (0.50)	0.58 (0.68)
	$\theta_{INST.}$(°)	57 (19)	2 (25)

[a] Numbers in parentheses are 1 σ uncertainties.

3.3 *Planetary Determinations*

The next brighter 1300 μm sources after Orion are the planets. Generally, the four planets Venus, Mars, Jupiter, and Saturn are bright enough to be useful polarization probes. However, Mars is usually small and weak and Venus is always near the Sun, reducing the usefulness of these two planets. We did observe both planets in 1989 and Venus in 1988, but because of their lower fluxes or poor sky positioning near the Sun little effort was focused on these planets, and only poor parallactic angle tracks were obtained. The 12-meter telescope also suffers from Sun-induced gain changes at 1300 μm (as deduced from our 1989 planetary observations). Hence, our best estimates for instrumental polarization come from Saturn observations in 1988 and Jupiter in 1989, both of which were observed during the nighttime when the telescope surface was thermally stable. It would have been preferable to compare the *same* planet for the two years, but that was not possible: Saturn was a daytime object in January 1989, and Jupiter was a daytime object in April 1988. The higher continuum flux of Jupiter in 1989 led to estimates of the instrumental polarization which are factors of 5–7 more precise than the Saturn 1988 data, as shown below.

Table 3 summarizes the Saturn 1988 and Jupiter 1989 least-squares fitting to the run of observed U and Q parameters with parallactic angle for Saturn in 1988 and Jupiter in 1989. Since the 1988 channel-V data agreed so closely with the channel-H data, we infer that no ADC saturation occurred and will utilize the V-channel data. The first item to note is that no polarization due to Saturn was detected. However, for Jupiter, significant polarization was detected in both the H channel (3.5σ) and the V channel (5.3σ). Also, although the percentage polarizations in H and V differ at almost the 2σ level, the position angles are only 1σ different, independently verifying the Jupiter detection. Further discussion of the details of the Jupiter detection is contained in Section 4 below.

TABLE 3

Planetary Instrumental Polarization

Year/Planet	Quantity	Channel *H*	Channel *V*
1988	P_{SOURCE}(%)	0.07 (0.05)[a]	0.03 (0.06)
Saturn	θ_{SOURCE}(°)	7 (18)	−15 (32)
	$P_{INST.}$(%)	0.13 (0.05)	0.21 (0.06)
	$\theta_{INST.}$(°)	28 (10)	64 (8)
1989	P_{SOURCE}(%)	0.028 (0.008)	0.063 (0.012)
Jupiter	θ_{SOURCE}(°)	−90 (8)	−76 (5)
	$P_{INST.}$(%)	0.185 (0.008)	0.097 (0.012)
	$\theta_{INST.}$(°)	52 (1)	71 (4)

[a] Numbers in parentheses are 1 σ uncertainties.

The derived main-beam instrumental polarizations for 1988 and 1989 were significantly detected (~3σ for 1988, ~10σ for 1989) and are also reasonably similar in percentage and position angle. But because the optical paths for the receivers H and V are not quite identical (one has an added reflection produced by another wire grid), and because the characteristics of the individual feed horn and mixer combinations could affect their polarization response, it is inappropriate to average the data of Table 3 between the channels. Instead, we adopt the instrumental polarization measured for Saturn in 1988 for channels H and V to correct all of the data for that year. Similarly, the Jupiter 1989 values have been used to correct the 1989 data.

The uncertainties associated with these corrections are roughly 0.06% for 1988 and 0.01% for 1989. Hence, astronomical detection of significant polarization must exceed roughly three times these values, or 0.18% for 1988 and 0.03% for 1989 to be considered significant, independent of the internal uncertainties of the source polarizations.

In order to verify that pointing errors would not lead to large induced polarizations, we needed to show that the telescope main beam was only mildly polarization sensitive on small angular scales. This was a much tougher criterion than that used in the previous determinations of instrumental polarization, where beam-averaged results were quoted. If various portions of the telescope main beam are highly polarization sensitive, then beam-averaged results showing low instrumental polarization might not be sufficient.

A four-position map of the telescope beam using Jupiter was made in 1989 by offsetting the telescope beam by one Jupiter radius (22″) in each cardinal direction. Since long parallactic angle tracks were not obtained, it was not possible to use the least-squares rotation method used above to separate the source and instrumental polarizations. Also, in order to boost the signal-to-noise ratio, the data from channel H and channel V were averaged. The results are listed in Table 4. The first column lists the position angles of the telescope positions relative to the center of Jupiter. The second column lists the percentage polarizations and uncertainties obtained at those positions. The last column lists the derived polarization position angles and uncertainties. These data include corrections for the polarimeter offset angle and parallactic angle rotation of Jupiter but do not include instrumental polarization corrections.

First, note that all of the polarization percentages are small (average = 0.24% ± 0.01%) and similar to the 1989 instrumental polarization values. Second, note that the percentages are highest, by almost a factor of two, for the equatorial telescope positions (90°, 270°). These positions are closer to being projected along the radiation zone of Jupiter than the polar positions (cf. de Pater and Dickel

TABLE 4

Jupiter Map

Position Angle (Degrees)	P (%)	θ (Degrees)
0	0.14 (0.02)[a]	86 (7)
90	0.25 (0.03)	75 (3)
180	0.18 (0.03)	60 (5)
270	0.36 (0.02)	54 (2)

[a] Numbers in parentheses are 1 σ uncertainties.

1986). Hence, we ascribe this increase to 1300-μm polarization from Jupiter (see below). Finally, there is a progression of position angles of the polarization as the telescope beam position angle changes. The mean position angle, 62°.7 ± 1°.5, is identically equal to the mean channel H and V instrumental polarization position angle. The almost sinusoidal excursion of the Jupiter polarization position angle with telescope position angle could represent modulation due to the nonsymmetric polarization distribution of the nonthermal radiation from the emission zones of the planet (see below). In any case, the beam map of Jupiter indicates that high polarization sensitivity of portions of the telescope beam was not present.

In Table 5 the measured instrumental polarizations for the main beam and sidelobes are summarized for the 1988 and 1989 observations for both receiver channels. Note that for the better-determined 1989 values, the derived position angles of the main beam and sidelobe polarizations are very similar. This is independent confirmation of the instrumental nature of these effects, as the main beam values come from Jupiter observations while the sidelobe values come from Moon observations.

4. Detection of 1300-μm Nonthermal Radiation from Jupiter

The lowest polarizations which MILLIPOL could measure were of the order of 0.03%, representing three times the uncertainty of the best main-beam instrumental polarization determination. However, that low limit depends on the certainty of the detection of polarized emission from Jupiter. If Jupiter were actually unpolarized, our separation of the Jupiter analysis into the two components, source and instrument, was incorrect. In that case the MILLIPOL polarization limit rises to nearly 0.6%, which is uncomfortably near the level of polarization detected in some of the massive cloud cores (Clemens *et al.* 1990).

In this section we establish the certainty of the Jupiter detection by comparing the polarized flux seen at 1300 μm to similar polarized fluxes at centimeter wavelengths

TABLE 5

Main Beam and Sidelobe Instrumental Polarizations

Year/Component	Quantity	Channel H	Channel V
1988	P(%)	0.13	0.21
Main Beam	θ(°)	28 (10)[a]	64 (8)
Sidelobes	P(%)	0.25	0.50
	θ(°)	113 (2)	98 (1)
1989	P(%)	0.185	0.097
Main Beam	θ(°)	52 (1)	71 (4)
Sidelobes	P(%)	0.50	1.0
	θ(°)	46 (2)	78 (1)

[a] Numbers in parentheses are 1 σ uncertainties.

and by comparing the corresponding polarization position angles. We further reinterpret the Jupiter beam map to independently confirm the Jupiter detection and to estimate the approximate polarized flux level away from the planet.

The low percentage polarizations detected for Jupiter in the two receiver channels (~ 0.04% average) correspond to about 1.5 Jy of polarized flux, a value of 50% higher than the detected polarized flux from Orion (BCL). Hence, although the polarized component of the radiation of Jupiter is very weak, it is not below the threshold for detection by MILLIPOL (that threshold is closer to about 0.10–0.25 Jy).

In Figure 3 the lower-frequency radio-polarization data compiled by Dickel, Degioanni, and Goodman (1970, hereafter DDG) for Jupiter are compared to our measurement. Since the thermal emission from Jupiter becomes very strong for frequencies higher than 10 GHz, and the polarization arises from the nonthermal high-energy electrons surrounding Jupiter, the percentage of polarized flux relative to total flux decreases strongly with frequency. Still, detection of a polarized component toward Jupiter is evidence for nonthermal emission. In the figure we have added a dotted line to indicate the trend fitted to log frequencies between 9 and 10.2. From extrapolation of the DDG work, polarized flux values at 1300 μm between 3 and 5 Jy are obtained. Our measured value is 1.5 Jy for the telescope beam pointed directly at Jupiter. However, our beam diameter, 30″, is significantly smaller than the beam sizes used to measure the lower frequency fluxes in the figure. Additionally, our Jupiter map indicates that polarized emission was extended with respect to the planet diameter. Hence, our polarized flux value for the central position is a lower limit for the polarized flux from the radiation belts, raising our point in Figure 3 by up to 0.9 dex (see below). Our polarized flux, and the assumption of a flat nonthermal spectral index, may be

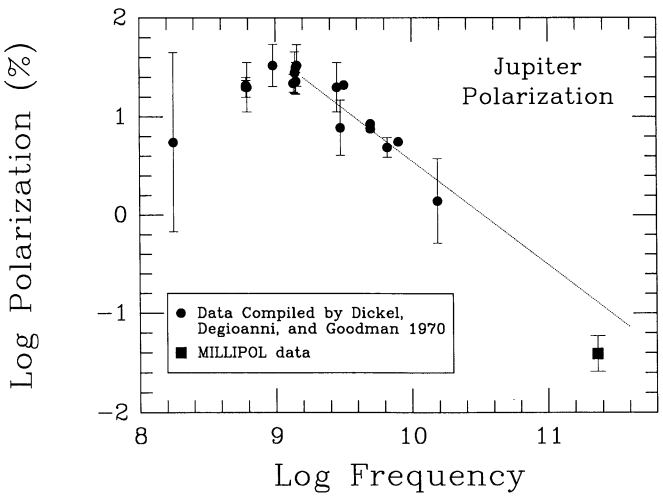

FIG. 3–Plot of the low-frequency percentage of polarized flux relative to total flux from Jupiter (from the compilation of Dickel *et al.* 1970) compared to our measured polarization at 230 GHz. The dotted line indicates the best-fit trend present in the low-frequency data between log frequencies of 9 and 10.2. The MILLIPOL data value is very nearly on this trend and represents a lower limit (see text).

used to estimate a fractional polarization for the 1300-μm nonthermal component between 35%–50%, similar to the values measured at centimetric wavelengths (60%–70%) by de Pater, Kenderdine, and Dickel (1982).

The data already presented in Table 4 indicated that the polarization is higher for equatorial regions toward the limb of Jupiter, which is consistent with the spatial distribution of the radio belts at longer wavelengths (de Pater and Jaffe 1984). If we correct the Jupiter map for the main-beam instrumental polarization, the excess polarization along the equatorial regions exceeds the polar regions by about a factor of five. Thus, to the limits of our measurements, the equatorial zone of Jupiter is coincident with all of the nonthermal emission detected at 1300 μm. The polarized flux associated with this equatorial zone far exceeds the average polarized flux detected directly toward the planet, by about a factor of eight. Since this number is computed from far fewer observations than the values reported in Table 3 we feel it is less certain.

Still, on three fronts, our Jupiter detection seems secure. The first test passed was that of the detection flux threshold—if polarized flux is present above 0.25 Jy, we ought to detect it. The second was the comparison of our polarized flux with lower frequency values from DDG. Finally, our Jupiter map shows polarized flux dominating in the same equatorial regions where the VLA has revealed lower-frequency, highly polarized nonthermal radiation belts.

5. Summary and Prospects

In this paper the present configuration of the MILLIPOL instrument was shown to consist of a rotating half-wave plate, tuned to 1300 μm, plus the analog signal processing electronics and computer support necessary to convert the coherent cooled receivers of the NRAO 12-meter telescope into a sensitive polarimeter. Design considerations of the analog and digital electronics were discussed and shown to have been optimized for our polarimetric applications.

Special care was given to accurate calibration and operation of the polarimeter. Among our calibration findings are the following:

- The Moon, Mars, Venus, and Orion observations all imply a main-beam instrumental polarization below 1%.
- Saturn and Jupiter measurements indicated nearly identical instrumental polarization values of $\leq 0.2\%$, with uncertainties as low as a factor of 20 smaller.
- Lunar observations established the sidelobe instrumental polarization sensitivity to be in the 0.25%–1.0% range.
- The polarization efficiency of the half-wave plate alone was measured to be roughly $95\% \pm 5\%$. Since there are no astronomical standard polarized sources at 1300 μm, the overall system polarization efficiency is unknown but probably not very different from the half-wave plate value.

Additionally, our calibration efforts led to the detection of polarized flux from the Jupiter system. A small map of Jupiter indicated that the polarized flux was strongest in the equatorial zone of Jupiter. Further, the amount of polarized flux is similar to that detected from the radiation belts of Jupiter at lower frequencies. We interpret our results to indicate that very close to Jupiter, predominantly along its equatorial zone, high-energy electrons continue to produce highly polarized nonthermal radiation at our observing frequency of 230 GHz.

Having demonstrated the sensitivity of this instrument and carefully calibrated the instrumental polarization, we have used MILLIPOL to probe the magnetic-field directions in several giant molecular cloud cores. In upcoming papers we will present our map of the Orion cloud core, obtained during 1988 and 1989 using MILLIPOL, in Leach *et al.* (1990), and a comparison of our detected polarization position angles and inferred magnetic-field directions for 5–7 other cloud cores in Clemens *et al.* (1990).

In the future we hope to use the MILLIPOL system at shorter wavelengths (~ 870 μm) and with bolometer detectors instead of coherent detectors. The shift to shorter wavelengths will lead to better angular resolution for polarimetric mapping. The use of bolometer detectors will greatly lower the current flux limit for detecting polarization in astronomical sources. The speed gain with such a system would allow surveying about 100 molecular cloud cores for 1% polarized thermal dust emission in only a few days of telescope time.

We wish to thank everyone involved in making the MILLIPOL effort possible. Special thanks go to Betty Stobie for software support at NRAO and for her emergency trip up the mountain on Easter day 1988 to write computer code to perform right-ascension switching on the 12-meter telescope. John Payne offered guidance and enthusiasm along with the ADC, multiplexer, and op-amp chips. This effort has been partially supported by a Flinn Foundation Grant of the Research Corporation, NASA grant NAG 51160, and by start-up funds from the Office of the Dean, College of Liberal Arts, Boston University, all to D.C. Partial NRAO support for travel to the telescope for R.B. is gratefully acknowledged.

APPENDIX

A Peek Under the Hood

In this Appendix we present a very detailed look at some of the specifics of the MILLIPOL electronics and computer systems and their interactions. This discussion includes a tour of the analog and digital signal processing chain and mention of how the computer was used to dynamically control the data collection.

A.1 *Electronics*

Figure 4 shows a schematic diagram of the analog signal processing chain for one of the two signal channels. This electronics chain had three functions. First it subtracted a reference voltage from the input signal and amplified the difference signal (at U1). Next, that difference signal was integrated during a short time interval (at U2). The integrated signal was then held while the analog-to-digital converter (ADC) converted the integrated difference voltage to a digital representation (12 bits). The differencing performed at U1 allowed good control of the system linearity over the large dynamic range ($\sim 10^6$) discussed in Section 2.2. By dynamically controlling the reference voltage differenced at U1, the full dynamic range could be realized without introducing large signal nonlinearities in the operational amplifiers.

For cost reasons, fast 16-bit ADCs and fast voltage-to-frequency converters were rejected in favor of a fast 12-bit ADC. To make up the total of the 16 bits sought, the remaining four bits of information were *sent* from the data-collection computer to drive the most significant four bits of a fast 16-bit digital-to-analog converter (DAC). The output of the DAC produced the voltage which was differenced with the input signal from the continuum receiver in the first operational amplifier (op-amp) U1. The result of the difference was scaled and integrated by the second op-amp U2. The op-amp gains were chosen to

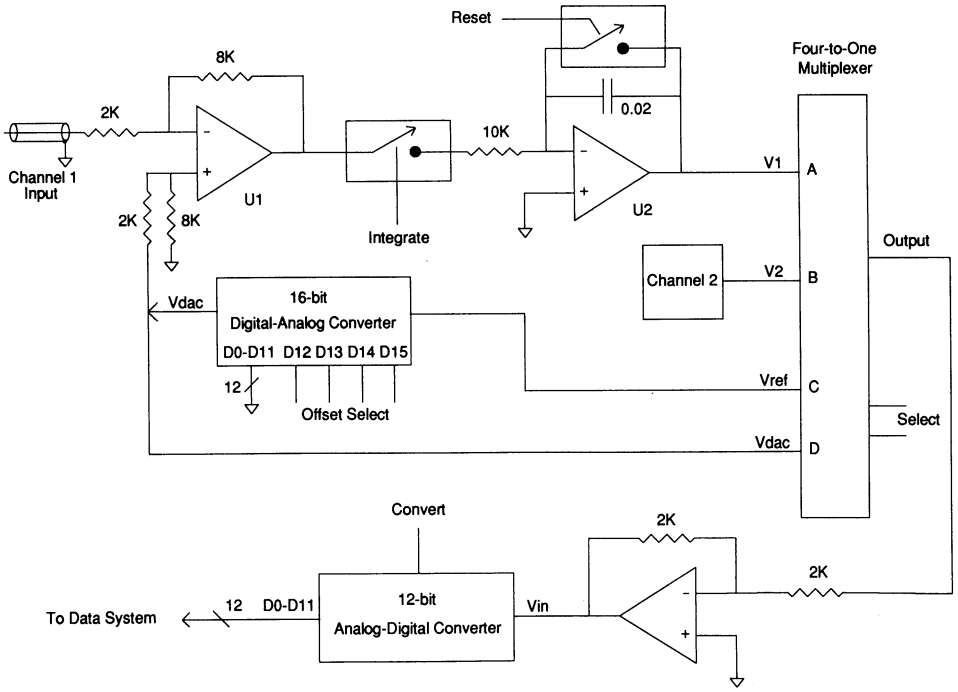

FIG. 4—Block diagram of the MILLIPOL analog signal processing electronics. The incoming detected continuum signal was differenced with the output of the Digital-to-Analog Converter (DAC) at U1. The difference signal was amplified and integrated at U2. The analog switches labeled "Integrate" and "Reset" were used to control the integration time window and to discharge the integration capacitor, respectively. (The two input channels have identical circuits U1 and U2. Only one channel is shown; the second channel is indicated as a box at the B input of the multiplexer.) The resulting integrated signal level was passed through an analog multiplexer to an impedance buffer and current driver before reaching the 12-bit Analog-to-Digital Converter (ADC). Computer commands were issued to discharge the integration capacitors, begin and stop the signal integration, control which signal channel or DAC voltage would be digitized, start the ADC conversion, and set the DAC offset voltage.

keep the signal level small compared to the op-amp voltage limits and large compared to the op-amp offset voltages. The gains were further chosen so that the op-amp integrated signal ADC range of 12 bits (~ 1 volt) could always be kept on scale for at least three consecutive DAC settings (step size ~ 0.25 volt). Thus, any input signal would be on-scale for both horizontal and vertical receiver channels even in the presence of up to 0.5–0.6 volt of difference between the detected receiver outputs. These ranges were not quite optimized during the 1988 observing run, leading to saturation of the ADC counts for some channel-V data. The DAC performance was monitored for stability by digitizing both the DAC output voltage and internal reference voltage generated on the DAC chip.

The conversion gains of the initial difference op-amp U1 and the integrator op-amp U2 were set to ensure no digitization error in the conversion chain. The voltage step corresponding to one ADC count was 260 μV. In order to reconstruct the actual continuum receiver output voltages, the 12-bit ADC measured voltages were added to the difference voltages injected by the DAC. The resulting conversion gain was about 20 digital counts per Kelvin of receiver temperature. For a normal 800-μs integration using a 400K DSB receiver temperature (including insertion loss due to the half-wave plate), the noise expected was somewhat less than 30 digital counts. In the computer, the ADC counts were integer added for the five samplings taken during five consecutive 1°8 steps of the half-wave plate. Next, the computer performed double-precision floating point accumulation of the multiple samples comprising a single observation. This careful attention to the ADC resolution and data handling ensured that the ADC digitization noise was far below the noise in the weak polarization signals, even for deep multiscan averages.

During operation of the analog electronics system, computer commands were decoded by digital logic inside the analog electronics box to produce specific actions (e.g., integrator reset, signal hold, multiplexer signal input change, and ADC conversion start). Software timings were adjusted and checked with a fast oscilloscope to levels of 10 ns. A PROM-based logic sequencer in the analog electronics box also sent fixed command strings to simulate computer control. In this fashion, a voltmeter-like mode was available for checkout independent of the instrument control computer.

The overall efficiency of the analog electronics, defined as the fraction of real time spent integrating the signal on the integrating capacitors to the total time, was measured to be 91% for 1-ms dwell times and estimated to be 89% for 800-μs cycles. The largest source of dead time was the 25-μs conversion time of the ADC. Two such conversions occurred for each cycle, to digitize the two continuum receiver channels. The remaining 38–40 μs were allocated to various settling times of the analog switches and the multiplexer and to the discharge time of the integrating capacitors. The polarizer plate stepper motion commands were issued during the signal ADC conversion dwell times.

Another digital electronics system, also embedded in the analog processing electronics, monitored the status of the half-wave plate (to commanded *versus* actual plate rotation angle), indicated the telescope status (source or reference telescope position, telescope position error, receiver phase-lock-loop status), and showed a real-time display of the ADC counts.

A.2 *Computer*

The data-collection computer, a Motorola MVME133 68020-based monoboard computer, was responsible for issuing the low-level commands needed to control the analog signal processing. The computer also monitored the resulting ADC count levels to determine if a change of the DAC offset voltage level was needed. Generally, for an astronomical observation, the source brightness level was far smaller than the receiver and sky-noise levels. Also, the polarization percentages were typically very small (≤ 1%). Thus, once the proper DAC level was chosen by the computer, such that the resulting ADC counts were roughly midscale of their 12-bit range, the DAC did not need to be reset until the telescope elevation had changed enough to significantly change the analog input voltage level. However, for observations of the Moon and the calibration chopper, the source brightness was comparable to the receiver noise and the resulting source and reference signal voltages were very different. For this special case, the computer software performed DAC autoleveling (resetting the DAC until the ADC was on scale) for *each* source and reference observation.

The computer operated over a VME-bus to communicate with a crystal-controlled interrupt clock and a 16-bit parallel data bus to the analog electronics box. The interrupt service routines needed to drive the half-wave plate and the analog electronics were written in assembly language and integrated into the computer real-time operating system (VERSAdos). The resulting performance increase over the VME/10 used by BCL allowed the faster data-collection rate. Additionally, the computer simultaneously processed a FORTRAN program to collect and average the polarization data.

A typical observation using MILLIPOL consisted of five minutes of total integration time, spent as five separate 30-second observations in the source and reference telescope positions. Thus, 1.5 megabytes of data were collected by the computer for each such scan. The FORTRAN data-collection program binned the polarimeter data into 40 discrete angular bins and maintained a first-in-first-out (FIFO) buffer for updating the bins. The

FIFO was needed because telescope status (receiver lock, telescope pointing error) bits to the VME computer were updated *after* the data were collected only every 0.1 s by the PDP11 computer controlling the 12-meter telescope. Once a scan was successfully completed, the 40-bin count averages were converted to actual receiver voltages, as discussed above, and their values stored to disk.

REFERENCES

Barvainis, R. E. 1984, Ph.D. dissertation, University of Massachusetts, Amherst.

Barvainis, R., Clemens, D. P., and Leach, R. 1988, *A.J.*, **95**, 510 (BCL).

Clemens, D. P., Barvainis, R., Kane, B., and Leach, R. 1990, in preparation.

de Pater, I., and Dickel, J. R. 1986, *Ap. J.*, **308**, 459.

de Pater, I., and Jaffe, W. J. 1984, *Ap. J.*, **54**, 405.

de Pater, I., Kenderdine, S., and Dickel, J. R. 1982, *Icarus*, **51**, 25.

Dickel, J. R., Degioanni, J., and Goodman, G. 1970, *Radio Sci.*, **5**, 517 (DDG).

Dragovan, M. 1986, *Ap. J.*, **308**, 270.

Hagfors, T. 1970, *Radio Sci.*, **5**, 189.

Heyer, M. H., Vrba, F. J., Snell, R. L., Schloerb, F. P., Strom, S. E., Goldsmith, P. F., and Strom, K. M. 1987, *Ap. J.*, **321**, 855.

Hildebrand, R. H., Dragovan, M., and Novak, G. 1984, *Ap. J. (Letters)*, **284**, L51.

Leach, R., Clemens, D. P., Barvainis, R., and Kane, B. 1990, *Ap. J.*, submitted.

Novak, G., Gonatas, D. P., Hildebrand, R. H., and Platt, S. R. 1989*a*, *Pub. A.S.P.*, **101**, 215.

Novak, G., Gonatas, D. P., Hildebrand, R. H., Platt, S. R., and Dragovan, M. 1989*b* *Ap. J.*, **345**, 802.

Werner, M. W., Davidson, J. A., Morris, M., Novak, G., Platt, S. R., and Hildebrand, R. H. 1988, *Ap. J.*, **333**, 729.